IAC-25,B2,IP,29,x94524

Cube1G: a full-hemispherical, high-speed optical communication terminal for CubeSats

Lukas Rupert Rodeck^a, Fabian Rein^a, René Rüddenklau^a, Olman Quiros Jimenez^a, Hannes Zeihsel^a, Jan Paul Jakobs^a, Paul Gagern^a, Marc Frederic Drenhaus Coll, Jan Hildebrand^a, Markus Lang^a, Michael Kluge^a, Elisa Garbagnati^a, Marie-Theres Hahn^a, Benjamin Rödiger^a, Christopher Schmidt^a, Jorge Rosano Nonav^{a*}

Abstract

The growing demand for high-speed free-space optical satellite communication requires compact designs that operate independently of satellite attitude constraints. Cube1G, developed by the German Aerospace Center (DLR) Institute of Communications and Navigation (IKN), is a novel laser communication terminal that combines coarse and fine pointing mechanisms, allowing hemispherical beam steering independent of the satellite's orientation. With a compact volume of two units plus a "tuna can", Cube1G is designed for a wide range of missions, including satellites with limited attitude control, such as CubeSats, Earth observation platforms with strict payload orientation needs, and high-data-rate communication networks. The system supports 100 Mb/s inter-satellite links and 1 Gb/s space-to-ground connections. Its first in-orbit demonstration on the SeRANIS mission in 2026 will validate its performance and enhance the satellite's data transfer capabilities for scientific and operational payloads. This paper presents the design of the Cube1G terminal, expected in-orbit performance, and results from ground-based tests and qualification before its integration on the ATHENE 1 small satellite. Cube1G aims to support the development of flexible optical communication architectures and advance toward the next generation of satellite networks.

Keywords: CubeSat, free-space optical communications, coarse-pointing assembly, new space

1. Introduction

The modern space economy is built on data driven by the growth of small satellite constellations in both number and capability. The flood of information exchanged from orbit—from high-resolution earth imagery to high-throughput communication satellites—is pushing traditional radio frequency systems to their physical limit. These developments are making free-space optical communication (FSOC) less of a novelty and more of a necessity. For many satellite developers, only laser links can offer the bandwidth needed to realize the full potential of their constellations [1,2].

A dynamic market has risen to meet this demand for laser communication terminals (LCTs) [3,4,5]. Yet, a common bottleneck limits most of these solutions: they are fixed to the satellite's body and only offer a small field of view. This design imposes a significant operational constraint requiring the entire satellite to maneuver to establish and maintain a communication link. A solution is to use a steerable optical pointing assembly, such as a gimbal or Risley prisms. At the industrial scale, gimbaled terminals like Tesat-Spacecom's SCOT80, Mynaric's CONDOR Mk3 [6], and Blue Cubed's Cobalt [7] are becoming the workhorses of large government and commercial constellations on small satellites. At the other end of the spectrum, the CubeSat world has seen its own

breakthroughs. One notable example is the Laser Crosslink Experiment (LaCE) mission. The core technology developed by CACI, the Skylight terminal, is a compact, actively steered laser communications terminal that provides $\pm 50^{\circ}$ beam steering in a 1.5U form factor. This technology was demonstrated in orbit in 2024 on two 6U CubeSats [8].

To further enhance the operational flexibility and efficiency of CubeSats, the German Aerospace Center (DLR) has developed the CubelG LCT. Its primary innovation is a two-stage pointing system, which combines a coarse pointing assembly (CPA) for hemispherical coverage with a high-precision fine pointing assembly (FPA) for link stabilization. This architecture allows the terminal to track an optical ground station (OGS) or another satellite independent of the satellite's orientation. Cube1G offers a 1 Gb/s downlink and 100 Mb/s uplink in a compact volume of 2U plus an external optical head. Although it is also capable of supporting 100 Mb/s inter-satellite links (ISLs), its first in-orbit demonstration on the SeRANIS mission in 2026 will focus exclusively on its direct-to-Earth (DTE) capabilities. This paper presents the design, qualification, and ground-based test results of the CubelG terminal before its delivery and integration on the ATHENE 1 satellite.

^a Institute of Communications and Navigation, German Aerospace Center (DLR), Münchener Str. 20, 82234 Weßling, Germany

^{*} Corresponding Author: Jorge Rosano Nonay (e-mail: jorge.rosanononay@dlr.de)

2. System Design and Integration

This chapter describes the design of the Cube1G LCT, including an overview of its key subsystems and the terminal's integration process.

2.1. Cube1G Architecture and SeRANIS project

Cube1G is the latest development in DLR-IKN's modular approach to miniaturized LCTs, building on the Optical Space Infrared Downlink System (OSIRIS) program [9]. Its optomechanical assembly is inherited from OSIRIS4CubeSat, an optical downlink terminal demonstrated successfully an end-to-end transmission from a CubeSat to ground in 2023 [10,11]. CubeISL, shown in Fig. 1, further advances this technology, incorporating optical downlinks at 1 Gb/s, and uplinks and ISLs at 100 Mb/s over distances up to 1,500 km. To achieve a higher degree of autonomy, it integrates its own computing subsystem, reducing its dependency on the host satellite. Despite its small 1U form factor, the LCT relies on the host satellite's attitude and control system to perform the precise pointing necessary for establishing optical links [5].

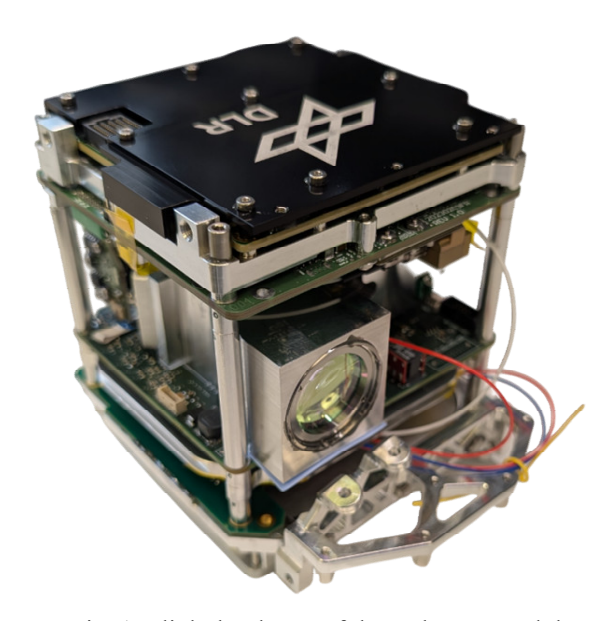


Fig. 1. Flight hardware of the CubeISL module

By building upon CubeISL LCT, Cube1G extends the terminal with a CPA, allowing it to operate independently of the satellite's attitude. Its independent beam-steering capability is crucial for developing future mega-constellations by enabling parallel optical communications and spacecraft operations on a CubeSat platform. The LCT uses a periscope to align the optical axis of the CubeISL module and the CPA. The flight hardware for all three modules is shown in Fig. 2.

The Cube1G LCT was initially designed and developed to combine an FPA, which consists of a fast-steering mirror (FSM) for precise pointing and tracking within a ±1° range and a CPA for coarse pointing across a hemispherical field of regard (FoR). However, for its demonstration mission, Cube1G will fly without the FPA. As detailed in *subsection 3.1.2*, this change was a result of the FSM's failure during vibration tests, which were subjected to high random vibration loads of 16.61 g_{RMS}. The modular design approach of both the Cube1G and CubeISL terminals allowed for the microelectro-mechanical system (MEMS) FSM to be replaced with a fixed mirror late in the development process. In this revised configuration, the CPA handles both coarse pointing and precise tracking.

The Cube1G terminal will be demonstrated as part of the Seamless Radio Access Networks for Internet of Space (SeRANIS) project led by the University of German armed forces in Munich (UniBw). SeRANIS is a small satellite mission designed to serve as a publicly accessible, multifunctional experimental laboratory. It supports research and development in key areas such as communication, navigation, artificial intelligence, and modern operations [12]. The satellite, ATHENE 1, is being built by OHB LuxSpace and has a mass of approximately 250 kg, including 90 kg of experimental payloads.

As part of the SeRANIS project, UniBw is also investigating optical space-to-ground communications for defense applications. To this end, they contracted DLR-IKN to develop an LCT for the ATHENE 1 small satellite. Given the large number of experiments on board, a primary requirement was the ability to perform a 1 Gb/s downlink independently of the satellite's attitude. The terminal should also be compliant with the Consultative Committee of Space Data Systems (CCSDS) optical on-off-keying (O3K) standard [13]. While flying on a small satellite, the LCT should also be CubeSat-compatible. Although the CubeISL LCT meets most of these requirements, it necessitates the satellite to maneuver to the link's target with a precision of less than 1° [5]. Therefore, the Cube1G LCT was developed to advance the CubeISL design with a new CPA. The ATHENE 1 satellite, carrying Cube1G, is scheduled to launch in Q3 2026 into a Sun-synchronous orbit (SSO). Operations will be managed by the German Space Operations Center (GSOC), with commissioning supported by DLR-IKN at the optical ground station in Oberpfaffenhofen (OGSOP). UniBw will conduct future operational downlinks with other optical ground stations to demonstrate the interoperability of FSOC.

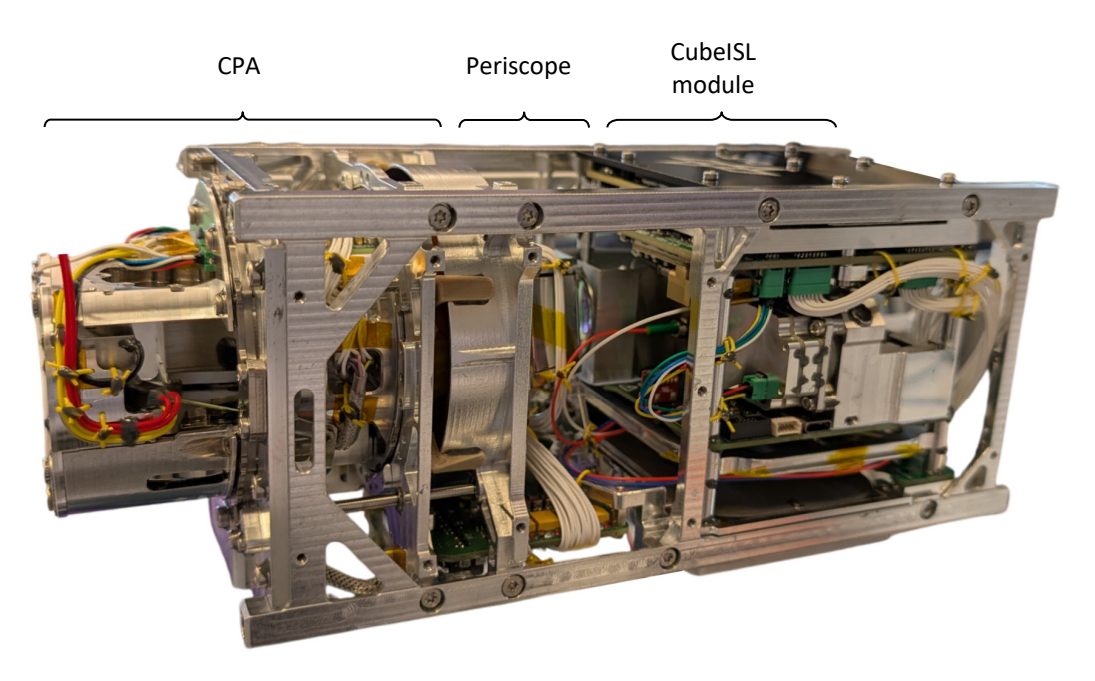


Fig. 2. Flight hardware of the Cube1G LCT and its three modules

2.2. Subsystem design

This section outlines the design of the optomechanical, electrical, and software subsystems. Fig. 6 shows a block diagram of the Cube1G LCT, comprising its three main modules—CPA, periscope, and CubeISL—along with their subsystems and the interface to the satellite. It also depicts the three stages of the CPA: stator, azimuth (Az), and elevation (El).

2.2.1. Mechanical and optical design

The mechanical and optical design of Cube1G is based on the strategic reuse of proven systems, such as the CubeISL LCT [5] and a prism-based CPA architecture [14]. This approach streamlined the development process, requiring only a minor adaptation of the existing optical terminal and setting the focus on the development of the CPA.

As shown in Fig. 2, the three main subsystems—the CPA, periscope, and CubeISL module—are bolted to a custom EN AW 7075-T7351 2U+ CubeSat structure. While this modular approach is beneficial, it also introduces trade-offs. The CubeISL terminal is designed for the standard PC104 hole pattern of the CubeSat Design Specification [15], but its aperture is offset from the central axis of the CubeSat and the CPA's optical path [5]. To correct this, a three-component periscope was introduced between the CubeISL and CPA to ensure translational alignment of the beam. The periscope consists of two RSA6061 aluminum mirrors glued to an aluminum structure made from a CTE-matching alloy.

The payload's optical head occupies a Ø 64 mm cylindrical volume protruding from the main structure, called "Tuna Can". For the SeRANIS mission, a dedicated mechanical and thermal interface was developed to mount the Cube1G payload onto the larger ATHENE 1 satellite bus, as shown in Fig. 10.

Fig. 3 illustrates a simulation of the Cube1G optical design. The CPA's custom optical prism is made from the high-index dense flint glass N-SF66 to reduce its physical size while maintaining a >20 mm clear aperture compatible with the optical terminal. To further reduce the assembly's size, the prism's elevation axis is offset from its center of mass by 2.5 mm. The prism's lateral surfaces are tilted by 2° to prevent internal reflections from interfering with the optical signal.

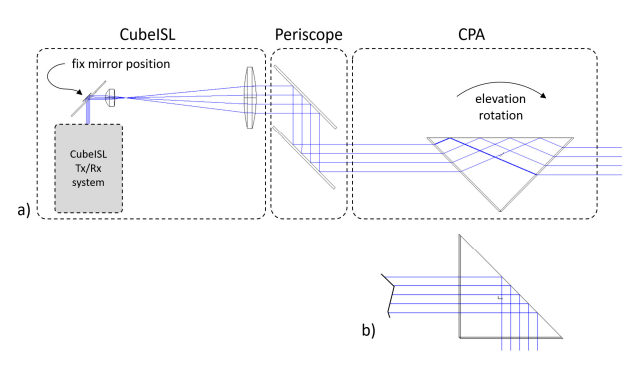


Fig. 3. a) Cube1G optical system pointing to nadir, b) prism rotated by 45°

In the initial design, the system included an FSM. However, for the SeRANIS mission configuration, it was replaced with a 7 mm commercial-off-the-shelf (COTS) fixed mirror installed at the same position. Further information regarding the CubeISL transmit (Tx) and receive (Rx) system can be found in [5].

The CPA itself is composed of three main subassemblies, detailed in the exploded view in Fig. 4. To achieve a full hemispherical FoR, the prism is housed in an elevation stage that rotates on a pair of ball bearings, actuated by a brushless DC (BLDC) motor, and monitored by a 26-bit absolute encoder. A motor driver with field-oriented control is used to control the motor. This elevation assembly is mounted on the azimuth stage, which features an identical bearing, motor, and encoder system to provide rotation relative to the stator assembly. Both axes are secured during launch by pin puller mechanisms, which are released upon commissioning in orbit.

The stator stage comprises all components fixed to the spacecraft structure, e.g., the 2U+ CubeSat structure or the CubeISL module. To reduce development complexity and component lead times, COTS components were used extensively, including BLDC motors, motor drivers (CAP-CORE SPI, Novanta Technologies), encoders (RESOLUTE UHV 52Dia/75Dia, Renishaw), ball bearings, and launch locks.

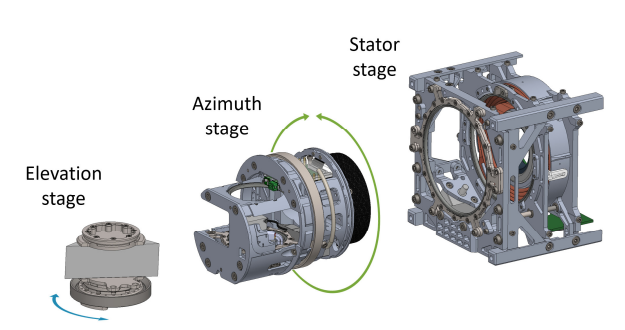


Fig. 4. Explosion view of the CPA

A novel, adjustable ball bearing preloading system was developed to ensure operational reliability after exposure to intense launch vibrations. Furthermore, a custom twist capsule was integrated into the stator stage to interface the El and Az PCBs [16, 17]. This capsule uses a flexible printed circuit (FPC) cable that wraps and unwraps between an inner and outer drum, allowing for >360° of continuous rotation, while leaving the central axis clear for the optical beam.

Cube1G is constructed primarily from aluminum alloys, with stainless steel fasteners, and selected titanium components for critical optomechanical interfaces. The use of exotic materials like beryllium

was not necessary to meet the mass and stiffness requirements. The total mass of the payload is 2576 g for the SeRANIS mission and 2300 g for a standard CubeSat configuration.

A thermal finite element analysis (FEA) was conducted to verify that critical components, such as the DHU and EDFA, remain within their operational temperature limits. Instead of performing a structural FEA on the bearing system, the design's resilience to launch loads was validated directly through a comprehensive vibration test campaign.

For data reception, the terminal features a direct detection receiver frontend (RFE) with an InGaAs avalanche photodiode (APD) [18]. The APD RFE is a custom development optimized for use in a miniaturized satellite. Fig. 5 showcases the RFE's compact size. Its control circuits are implemented as analog circuits, and it does not contain any programmable devices, which makes it less susceptible to radiation effects. The RFE operates autonomously, requiring no commanding or configuration. It uses a single interface for all necessary signals, including power, status, and data.

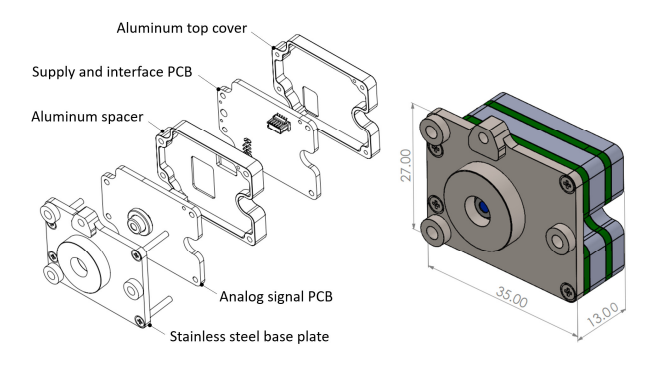


Fig. 5. Explosion view of the APD RFE

The transmitter system on the CubeISL module consists of a COTS seed laser and erbium-doped fiber amplifier (EDFA) [5]. The seed laser modulates LVDS downlink data on a 1553.3 nm (195.1 THz) on-off keying (OOK) fiber-coupled optical signal. This 1 mW signal is then amplified to 1 W by the EDFA before being collimated by the optical block. Although the seed laser supports a 10 kHz analog beacon input for ISLs, this function is not used in the SeRANIS project.

2.2.2. <u>Electrical design and interfaces</u>

The terminal's electrical and power architecture is distributed across seven primary functional subsystems:

- Data handling unit (DHU)
- Seed laser
- Optical amplifier (EDFA)
- CPA

- APD RFE
- Optical block
- Master attitude controller (MAC) [19]

To efficiently interconnect these subsystems (see *subsection 2.2.3* for further information on the DHU and MAC), a dedicated power distribution and control interface (PDCI) daughterboard was developed [19]. The PDCI features a power distribution system with latching current limiters (LCL) and multiple switchable power channels. This design allows the DHU to individually enable or disable every subsystem, depending on the operational mode. All subsystems are powered directly by the main bus voltage of 28 V and include their own internal voltage regulators to derive their specific operating voltages. Fig. 6 provides a block diagram of the subsystems and their power distribution.

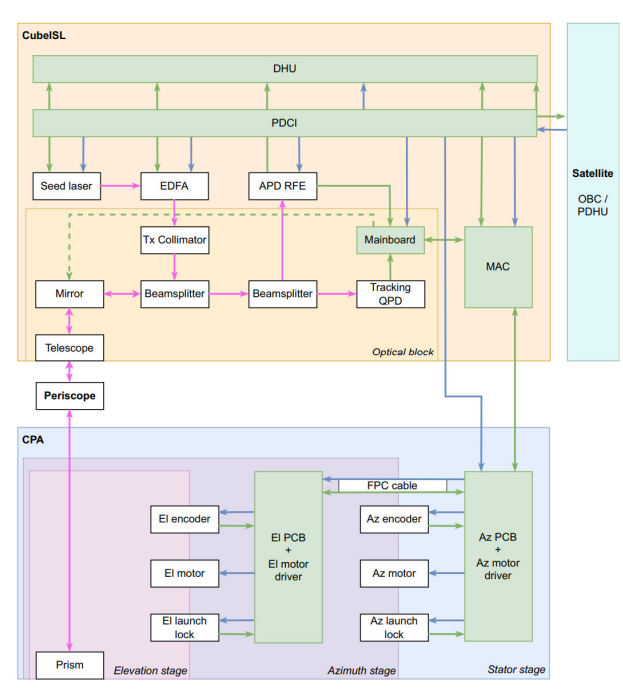


Fig. 6: Block diagram of the Cube1G LCT. Power, telemetry, and optical signals are represented by blue, green, and pink lines, respectively.

The power input from the satellite bus is protected by a separate LCL, which protects against overcurrent, undervoltage, and overvoltage. This is achieved using two types of metal-oxide-semiconductor field-effect transistor (MOSFET) switches: a standard low-current switch for most subsystems and a high-power switch specifically for the high-current EDFA.

The PDCI also manages both internal and external electrical communication interfaces. The terminal features a 1 Gb/s Ethernet interface for user data and

telemetry/telecommands (TM/TC), and a dedicated RS422/RS485 interface for auxiliary TM/TC.

The CPA electronics consist of an Az and an El PCB. Each board contains its motor driver, encoder readout circuitry, and power distribution. The Az PCB additionally houses a common launch lock actuator. To allow for relative motion between the axes, the boards are connected by a flexible, ~1-meter, two-layer FPC harness, wrapped inside the CPA's twist capsule. The harness features a continuous ground plane for reliable power delivery and signal integrity. The motor drivers communicate via a shared SPI bus. Therefore, transmitting signals over the >1 m harness necessitated careful consideration of high-frequency effects, which are discussed further in *subsection 3.2.1*.

2.2.3. Software design

The terminal's software architecture is distributed across three main systems: the DHU, the MAC, and the Mainboard (MB), and connected via two UART interfaces. The COTS DHU uses a multiprocessor system-on-chip (MPSoC) with a Xilinx Zynq UltraScale+ field-programmable gate array (FPGA). The MAC and MB each feature an ATSAM v71 microcontroller.

Data Handling Unit (DHU)

The DHU acts as the primary interface between the spacecraft bus and the Cube1G payload. Its software is based on a custom Linux distribution and is organized into independent services, each with a specific function. The DHU uses the CubeSat Space Protocol (CSP) for transporting and routing TM/TC packages to the satellite. CSP is a well-established protocol in the small satellite community, designed for communication within distributed embedded systems. For file transfers, the Trivial File Transfer Protocol (TFTP) is implemented, allowing Cube1G to operate as either a client or server depending on the configuration. The system maintains synchronized time by using a pulse-per-second (PPS) signal, first received by the DHU and then forwarded to the MAC and MB for overall synchronization.

The DHU software is organized into several independent services, including a telecommand service, telemetry service, file transfer service, time synchronization service, and managers for the MB and MAC. An additional service, *cubeisld*, provides a Telnet server with a Command Line Interface (CLI) for monitoring and control. This service can also execute pre-stored test and operational scripts. For implementation, the *libs3* library [20] is used, which features a parameter management system that stores parameters in a hierarchical tree structure. This approach provides high scalability and simplifies the

organization of system parameters, while supporting both telemetry and configuration parameters to enhance system observability and controllability.

MAC and MB Control Architecture

The control architecture of previous missions was handled entirely by a microcontroller on the MB, which processed inputs from all sensors and actuators. This approach required frequent redesigns of the MB to accommodate the changing requirements of different missions. To solve this, the MAC was introduced [19]. The MAC's modular design allows for the high-level combination of low-level control loops from individual subsystems, making it possible to add or restructure tasks on fully developed systems. In Cube1G, this approach reduces future development efforts for new mission configurations and requirements, as the MB now only manages the optical block's control.

When preparing for a downlink, the DHU first sends the necessary parameters—including target ground station position, link start time, and duration—to the MAC. The MAC then pre-calculates the required target positions in the Earth-Centered Inertial (ECI) frame for the entire link duration, reducing the computational load during the actual downlink. During the downlink stage, the DHU forwards data from the satellite's attitude and orbit determination system (AODS) to the MAC. The MAC uses this data to compute the pointing direction so the CPA targets the ground station and finds its beacon.

During the initialization of an optical downlink, the quadrant photodiode (QPD), managed by the MB, is calibrated [21]. The MB continuously sends the MAC data on whether a beacon signal was detected and its offset from the center position. The MAC uses this feedback to refine its highest-level control loop.

3. Qualification and performance testing

This chapter describes the qualification and testing of the CubelG LCT, including the evaluation of the terminal's performance under mission-representative conditions.

3.1. Environmental qualification campaign

The Cube1G terminal was qualified following a New Space approach, similar to that used for the O4C and CubeISL terminals, in which the engineering qualification model (EQM) undergoes testing for ionizing radiation, vibration loads and thermal-vacuum (TVAC) cycles [22]. The proto-flight model (PFM), built to be identical to the EQM, is therefore considered capable of withstanding the environmental loads expected during the mission.

Following delivery of the payload to UniBw, the Cube1G PFM will also undergo vibration, electromagnetic compatibility (EMC), and operational TVAC cycles as part of an acceptance qualification campaign. Due to schedule constraints in the Cube1G development, only the radiation and vibration tests were performed on the EQM and the TVAC qualification will be carried out directly on the PFM during its acceptance tests. The procedures and results of the tests prior to delivery are presented in the following subsections.

3.1.1. Total ionizing dose

All electronic subsystems of the terminal underwent total ionizing dose (TID) qualification to ensure nominal functionality at end-of-life (EOL) under the LEO radiation environment. The TID qualification was performed at the Helmholtz-Zentrum Berlin (HZB) using a cobalt-60 gamma-ray source.

In addition to the EDFA that had been previously qualified for CubeISL [22], the following components were tested: MAC, MB, PDCI, Az PCB, APD RFE, motor driver, and encoder read-head. The expected TID for a five-year mission in a 600 km SSO was calculated with OMERE, resulting in 5 krad(Si) for an equivalent aluminum shielding thickness of 3.5 mm. The components were irradiated to 6 krad(Si) at a rate of 5.28 krad/h. No degradation in performance or loss of functionality was observed in any of the tested components. In particular, the APD RFE maintained the same bit error rate (BER) versus received optical power as before irradiation (see Fig. 9).

3.1.2. Random vibration

The primary objectives of the vibration qualification campaign were to verify the structural integrity of the Cube1G LCT EQM, identify its first structural natural frequency, and confirm the functionality post-vibration of all subsystems. Particularly of critical optical components and movable mechanisms, including the two-stage pointing system, launch locks, and the FSM.

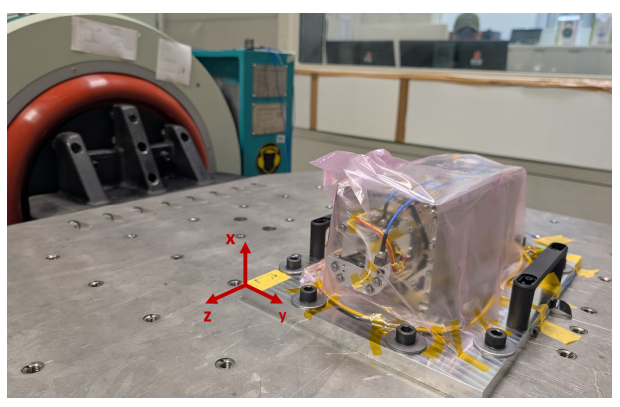


Fig. 7. Vibration qualification on Cube1G EQM

For the qualification, the EQM was subjected to a sequence of random vibration loads along each of its three orthogonal axes for one minute per axis. The tests were conducted at the shaker facility of the UniBw München. The test sequence progressed through three levels: (1) a 7.25 g_{RMS} load corresponding to Falcon 9 protoqualification standards, (2) an intermediate mission load of 10.50 g_{RMS} (SeRANIS mission specification reduced by 3.8 dB), and (3) the full SeRANIS mission load of 16.61 g_{RMS} , as shown in Fig. 8. Functional checks were performed between each test run.

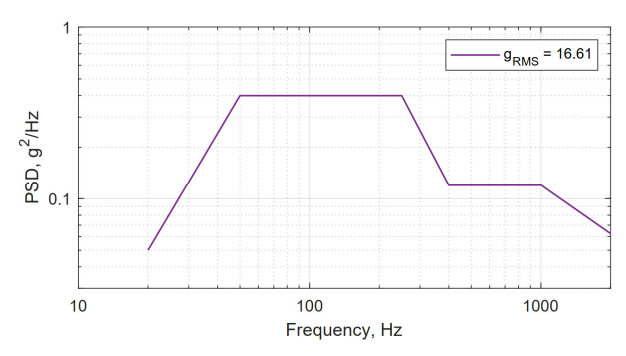


Fig. 8. Maximum predicted random vibration envelope for the SeRANIS launch

The vibration campaign revealed minor shifts in the LCT's natural frequencies, which were attributed to the settling of movable components. Table 1 shows a comparison of the LCT's first eigenfrequency before and after the qualification test for each axis. Functional tests confirmed that the mechanical structure sustained no permanent damage, successfully demonstrating its integrity up to the full mission load.

Table 1. First natural frequencies of the LCT before and after the vibration qualification

	Pre-shaker, Hz	Post-shaker, Hz
x-axis (height)	528	471
y-axis (width)	380	374
z-axis (length)	525	499

However, the campaign revealed performance degradation in specific subsystems under higher loads. While the LCT withstood without issues the 7.25 g_{RMS} Falcon 9 protoqualification loads typical for CubeSat payloads, failures were observed at subsequent levels. One axis of the FSM failed during the 10.50 g_{RMS} test, followed by a complete failure at the full 16.61 g_{RMS} load. Additionally, the pin puller for the Az launch lock became jammed after the 10.50 g_{RMS} test, requiring manual release. The pin puller did, however, operate normally after the final 16.61 g_{RMS} test. No other components exhibited performance losses.

The FSM failure was a critical issue, as it represented a single point of failure in the LCT's initial configuration. The ATHENE 1 launch on a Falcon 9 is expected to have lower vibration loads than the full qualification levels. However, the flight model must still pass acceptance tests at these high levels, which made the risk of FSM failure unacceptable. Consequently, a risk-reduction process was conducted, and a design modification was implemented. Leveraging the performance of the CPA and the flexibility of the MAC, it was analyzed and tested that mission objectives could be met without the FSM (as detailed in subsection 3.2.3). The FSM was therefore replaced with a fixed mirror, which is less sensitive to vibration and shock, and all pointing tasks were consolidated into the CPA. To address the jamming issue, the Az pin puller socket was also redesigned and lubricated with Fomblin Z25 to improve its operational reliability.

These findings must be contextualized within the mission's specific launch requirements. The Cube1G terminal was designed for CubeSat applications, and its successful performance at the 7.25 g_{RMS} Falcon 9 protoqualification level confirms its suitability for a standard launch inside a deployer. The failures occurred only at the higher qualification levels (i.e., 16.61 g_{RMS}) because, for this mission, the satellite will be hardmounted directly to the rocket structure. This configuration bypasses the vibrational damping of a deployer, exposing the terminal to a significantly harsher vibration environment than its original design specification. Therefore, the issues encountered were a direct result of these demanding, mission-specific requirements rather than an inherent design flaw for its intended use case.

3.1.3. TVAC cycles

As part of its acceptance qualification, the PFM will undergo a reduced TVAC test at a pressure of 10⁻⁵ mbar. The test profile consists of an initial bakeout, one nonoperational cycle from -20 °C to +80 °C, and four operational cycles from 0 °C to +60 °C. Each operational cycle will include a hot and a cold start following a non-operational dwell period. A full functional test will be performed during the first and last operational cycles, with reduced functional tests conducted on the two intermediate cycles. During the mission, the CPA will be directly exposed to space, with one surface receiving direct solar illumination while the others radiate towards deep space. This will induce a significant thermal gradient across the CPA (in x or y axes). To replicate these operational conditions, a sun simulator or a localized heater will be used to generate a thermal gradient during the final test cycle. This procedure is designed to verify that the two stages of the

CPA can function nominally under the expected range of temperatures and thermal gradients.

3.2. Performance and functional testing

The performance and functional integrity of the Cube1G PFM were validated through a comprehensive series of tests at both the subsystem and system levels. This section details the results from three key areas: the characterization of the electrical subsystems, the optomechanical assembly, integration, and testing (AIT), and the validation of the control loop and tracking performance.

3.2.1. <u>Electrical subsystem test results</u>

The power distribution system on the PDCI was optimized for efficiency by using MOSFET switches with low power loss. The high-power n-channel MOSFETs for the LCLs feature a measured onresistance below 2.5 m Ω , resulting in a power loss of 133 mW at the maximum current of 2.2 A. For lower-power channels, compact p-channel MOSFETs in SOT23-3 housings were employed, ensuring minimal power dissipation (i.e., 132 m Ω or <34 mW at 0.5 A) and maintaining thermal stability across the system.

The performance of the optical receiver is defined by its APD RFE. Benchtop characterization showed a sensitivity of approximately 800 photons/bit at a bit error rate (BER) of 10⁻⁴. This corresponds to a minimum detectable power of 10.25 nW for a 100 Mb/s signal at a wavelength of 1550 nm. Fig. 9 compares the RFE's sensitivity from the PFM's benchtop characterization, and for the EQM before and after the TID irradiation of 6 krad(Si).

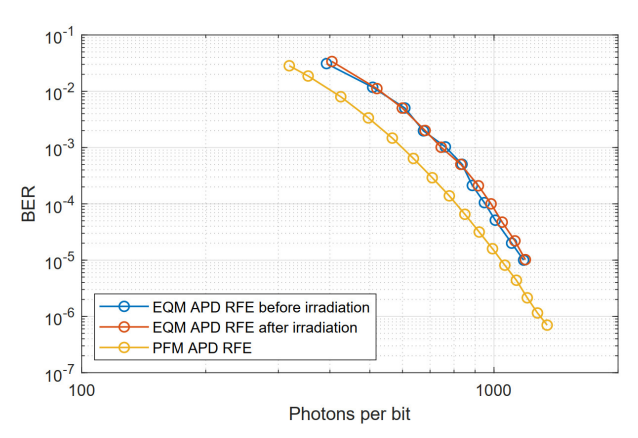


Fig. 9. Comparison of the APD RFE's sensitivity for the PFM and EQM pre- and post-irradiation

Regarding the twist capsule, it was a critical design challenge to ensure signal integrity through the ~1-meter flexible CPA harness for the SPI bus. A comparative study was performed between a standard flat flexible cable (FFC) and a custom two-layer FPC to

select the optimal solution. Time-domain reflectometry (TDR) tests clearly demonstrated the superiority of the FPC. The standard FFC, which has weak ground coupling and a discontinuous impedance profile, induced significant signal integrity issues such as ringing, plateaus, and ground bounce. The FPC, designed as a microstrip with a continuous ground plane, effectively mitigated these distortive effects and maintained stable communication. These findings were supported frequency-domain transmissivity measurements. While both cables showed strong attenuation around 50 MHz (a $\lambda/4$ effect corresponding to the trace length), the FFC exhibited increased attenuation and an additional notch at ~75 MHz.

3.2.2. Optomechanical integration and testing

The modular design of the Cube1G terminal allows an independent and parallel assembly of its two main subsystems: the CubeISL module and the CPA with its periscope. These are assembled during the final stages of the terminal integration.

The AIT procedure for the CubeISL module is nearly identical for all missions, with only minor mechanical differences at the side rail interfaces. The first step is the assembly of its optical block, which constitutes the core of the terminal's optical system [5]. For the SeRANIS mission configuration, which does not feature an FPA, an FSM is temporarily incorporated to simplify the calibration and alignment of the optical components. The telescope is collimated with the help of a shear interferometer by tuning the axially-adjustable front lens. The resulting spot size and shape are then measured at the QPD detector plane and validated against optical simulations [5].

Following the alignment of the primary optics, the detectors are integrated. The QPD is mounted first, and its tracking performance is characterized. The PFM system managed to acquire and track a ground station signal with a minimum input power of ~ 150 pW at the detector plane. This value, however, represents optimal laboratory conditions without background noise, where tracking stability is expected to be higher than for a nominal operational scenario [22].

Next, the APD RFE is co-aligned with the QPD using a custom-designed focal assembly. This mechanism uses two orthogonal fine-thread screws to precisely adjust the radial position of the focal assembly against a counteracting leaf spring. A locking screw secures the assembly once alignment is finalized. This setup allows the QPD and APD to be focused and aligned independently. The integrated APD RFE achieved a BER of 10⁻⁴ with an input power of 17 nW (1330 photons/bit) at its detector plane. The 2 dB power

loss observed relative to benchtop characterizations (Fig. 9) is attributed to transmission and coupling losses within the assembled optical system.

After the integration of the detectors, the temporary FSM is replaced with the fixed mirror. The Tx optical axis is then co-aligned with the Rx beam path using a gimbaled COTS fiber collimator located in the terminal's optical block. The final angular error of the PFM's Tx/Rx alignment is <19 μrad . For comparison, the LCT's theoretical full width at half maximum (FWHM) divergence is 105 μrad . Finally, the front telescope lens is readjusted to ensure collimation in vacuum, compensating for the difference in refractive index compared to air.

In the final step, the fully characterized CubeISL module is integrated with the CPA. The relative height and orientation between the two assemblies are precisely adjusted to center the Tx spot on the CPA prism. On the PFM, it was successfully aligned within 1.2 mm of its optimal position. Since the prism is 2 mm larger than the clear aperture of the optical block, this slight deviation does not truncate the optical beam. A final system-level check verifies the terminal's collimation, Tx spot quality, and Tx/Rx alignment, preparing the terminal for performance analysis of pointing, acquisition, and tracking (PAT).

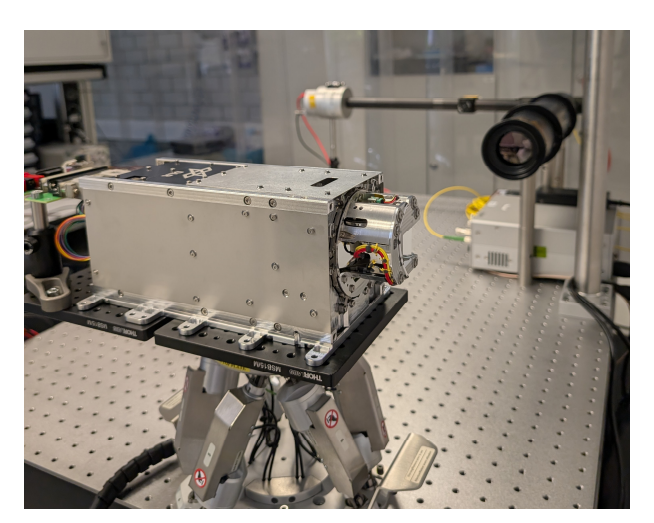


Fig. 10. Optical characterization of the PFM on the optical ground support setup

3.2.3. Control loop and tracking accuracy validation

The successful operation of the CPA relies on the precise tuning of the control loop of both axes to ensure a robust tracking performance, especially in the absence of an FPA. The controller's design balances tracking accuracy with system dynamics. To mitigate jitter and abrupt changes in acceleration, an s-curve profiler smooths the ephemeris-based trajectory data, achieving

a control error as low as 2 μrad for movements with a maximum velocity and acceleration of 0.001 rev/s and 0.1 rev/s² [23]. This performance is well-suited for the SeRANIS mission, where the satellite's attitude velocity during a ground link is expected to be <0.0024 rev/s, a rate comparable to the tested parameters. To handle different operational states, a gain-scheduling approach is used, applying distinct controller parameters for large-angle pointing maneuvers versus fine-tracking adjustments. This technique allows the use of different sets of controller parameters based on the system's operational state—e.g., for long-range maneuvers, where the system operates outside the stick-slip friction zone.

Before testing the system's PAT procedure, a calibration of the azimuth axis's rotation relative to the local coordinate system of the QPD was performed. This allows transforming any measured tracking errors within the QPD's local coordinate system into the CPA's current local coordinate system during operation. The closed-loop PAT performance was validated in a test where the CPA first executed a grid-spiral search pattern to find a beacon signal (see Fig. 11). Upon signal acquisition with the QPD at t=1737 s, the system switches to tracking mode, actively correcting misalignments based on QPD feedback.

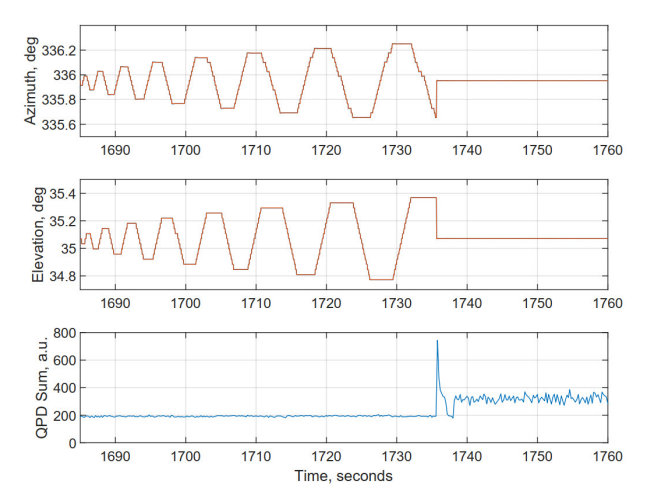


Fig. 11. PAT procedure of the Cube1G LCT

As shown in the close-up view in Fig. 12, the optical control loop is tuned for robustness and low steady-state error, consistent with the expected low-frequency disturbances of the mission. The results demonstrate excellent performance, with the internal CPA control error remaining below 6.5 µrad, with a mean of 2 µrad and a standard deviation of 1.2 µrad. This error constitutes a minor part of the overall system error measured by the QPD, which had a mean of 21 µrad and a standard deviation of 12.5 µrad. The residual error

is attributed to disturbances at frequencies above the controller's 20 Hz sampling rate. Because all tuning variables are parametrized, the controller's bandwidth can be readjusted on-orbit if necessary.

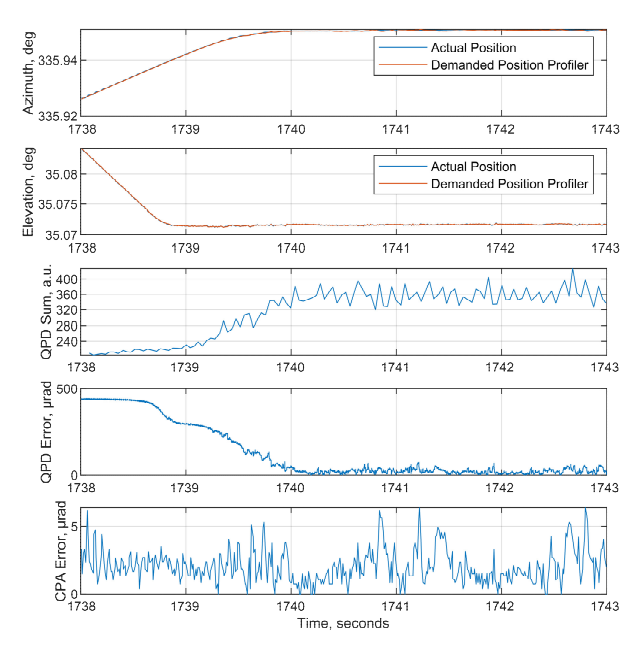


Fig. 12: Closed-up view of the mode switch between acquisition and tracking

Finally, successful PAT was demonstrated across a variety of pointing angles, including up to $4^{\rm o}$ from nadir, which validates the internal coordinate system derotation between the CPA and the QPD. The tests also verified the spiral pattern predistortion algorithm. This algorithm compensates for two key effects: the 2:1 mechanical-to-optical angle conversion for the El axis, and the reduced effectiveness of the Az axis at high elevation angles. The compensation factor for the Az axis was approximated as $1/\text{sin}(\theta_{el})$, where θ_{el} is the optical elevation angle.

4. Conclusion and next steps

This paper presents Cube1G, a compact LCT for CubeSats from the German Aerospace Center (DLR). Its key feature is a coarse pointing assembly (CPA) that provides full hemispherical coverage, allowing the terminal to operate independently of the satellite's orientation. The system is designed for a 2U plus "tuna can" volume and supports 1 Gb/s space-to-ground and 100 Mb/s inter-satellite links.

A critical design change involved replacing the fast-steering mirror (FSM) with a fixed mirror after the FSM failed at the highest loads of the vibration qualification (i.e., 16.61 g_{RMS}). As a result, all pointing and tracking tasks were consolidated into the more robust CPA. The proto-flight model (PFM) has been successfully

characterized and delivered to the UniBw for final acceptance tests and integration into the ATHENE 1 satellite. Cube1G is scheduled for its first in-orbit demonstration on the SeRANIS mission, with a planned launch in Q3 2026.

The LCT's development was closely aligned with our industrial partner, Tesat Spacecom, and their commercial CubeISL product line, marketed as the SCOT-20. This collaboration provides a direct path to commercialization following the planned in-orbit demonstration of Cube1G. An extension of the technology, the SCOT-30, is also being developed by Tesat and will feature a modified CPA with an increased 30 mm aperture. This close partnership allows DLR to focus on technology demonstration and adaptation for new mission concepts while Tesat the availability of a commercially ensures manufactured, high-quantity product.

In addition to LEO satellite missions, the versatile architecture of Cube1G is also highly suitable for airborne applications. High-altitude platforms (HAPs) and unmanned aerial vehicles (UAVs) present similar challenges to small satellites, requiring high-data-rate, agile communication links while facing strict size, weight, and power (SWaP) constraints. Cube1G's design and its interoperability with the commercial SCOT product family make it a key enabling technology for future high-performance, compact laser communication networks in both space and airborne domains.

Acknowledgements

This research work is funded by dtec.bw – Digitalization and Technology Research Center of the Bundeswehr – and has been supported partially by the German Federal Ministry of Defense through the technological research and development assignment "Responsive Space Capabilities". Dtec.bw is funded by the European Union – NextGenerationEU.

References

- [1] A. U. Chaudhry, H. Yanikomeroglu, "Laser Intersatellite Links in a Starlink Constellation: A Classification and Analysis," IEEE Vehicular Technology Magazine, vol. 16, no. 2, pp. 48-56, (2021).
- [2] J. Spicer, S. Lau, R. Aucoin, "Results of SDA-standard-compatible optical inter-satellite link testing between Kepler Communications LEO satellites," Proc. SPIE 13355, Free-Space Laser Communications XXXVII, 1335502, (2025).

- [3] T. S. Rose, D. W. Rowen, S. D. LaLumondiere, et al., "Optical communications downlink from a low-earth orbiting 1.5U CubeSat," Opt. Express 27, 24382–24392, (2019).
- [4] C. M. Schieler, K. M. Riesing, B. C. Bilyeu, et al., "TBIRD 200-Gbps CubeSat downlink: system architecture and mission plan," IEEE International Conference on Space Optical Systems and Applications (ICSOS), pp. 181–185, (2022).
- [5] J. Rosano Nonay, R. Rüddenklau, A. Sinn, et al., "Horizontal free-space optical link with CubeISL over 143 km," J. Opt. Commun. Netw. 16, 593-601, (2024).
- [6] O. I. Younus, A. Riaz, R. Binns, et al., "Overview of Space-Based Laser Communication Missions and Payloads: Insights from the Autonomous Laser Inter-Satellite Gigabit Network (ALIGN)," Aerospace 2024, 11, 907, (2024).
- [7] R. W. Kingsbury, J. C. Twichell, S. E. Palo, "Cobalt optical crosslink terminal," Proc. SPIE 11993, Free-Space Laser Communications XXXIV, 119930N, (2022).
- [8] S. Stanko, D. Frey, J. Ruvalcaba, et al., "Laser Crosslink Experiment: A Mission Overview," 38th Small Satellite Conference, (2024).
- [9] C. Schmidt, B. Rödiger, J. Rosano Nonay, et al., "DLR's Optical Communication Terminals for CubeSats," 2022 IEEE ICSOS, (2022).
- [10] B. Rödiger, C. Roubal, F. Rein, et al., "OSIRIS4CubeSat—The World's Smallest Commercially Available Laser Communication Terminal," Aerospace 2025, 12, 655, (2025).
- [11] B. Rödiger, C. Schmidt, "In-orbit demonstration of the world's smallest laser communication terminal: OSIRIS4CubeSat/CubeLCT," Proc. SPIE 13546, 4S Symposium, (2025).
- [12] S. Kaya, D. Tuzi, P. Agbo, et al., "Mobile networks expanding to space: overview of the SeRANIS beyond 5G testbed," ITU Journal on Future and Evolving Technologies, vol. 5 2, (2024).
- [13] B. L. Edwards, R. Daddato, K.-J. Schulz, et al., "An Update on the CCSDS Optical Communications Working Group," 2019 IEEE ICSOS, (2019).
- [14] B. Rödiger, L. R. Rodeck, M.-T. Hahn, et al., "Transformation of DLR's laser communication terminals for CubeSats towards new application scenarios" The 4S Symposium 2024, (2024).
- [15] PC/104 Embedded Consortium, "PC/104 Specification" Version 2.6, (2008).
- [16] K. A. Blumenstock, J. A. Niemeyer, J. P. Schepis, et al., "Flex-Capsules for the Roman Space Telescope High Gain Antenna Gimbal" 20th European Space Mechanisms and Tribology Symposium, (2023).
- [17] P.-A. Mäusli, G. Feusier, V. Gass, "Rotating electrical joints with continuous metallic

- connections" 10th European Space Mechanisms and Tribology Symposium, (2003).
- [18] D. Giggenbach, "Free-Space Optical Data Receivers with Avalanche Detectors for Satellite Downlinks Regarding Background Light" Sensors, vol. 22, no. 18, (2022).
- [19] R. Rüddenklau, H. Zeihsel, F. Rein, et al., "Master attitude controller for modular laser communication systems", IFAC Workshop on Control Aspects of Multi-Satellite Systems, (2025)
- [20] O. Quiros Jimenez, "The S3 Project libs3pp" GitHub repository https://gitlab.com/s3space/libs3pp, commit 6cb9540fcbc3df6f25bdf308283a7343f3eeef6a, (2024).
- [21] R. Rüddenklau, F. Rein, C. Roubal, et al., "In-orbit demonstration of acquisition and tracking on OSIRIS4CubeSat" Optics Express, vol. 32, no. 23, (2024).
- [22] B. Rödiger, J. Rosano Nonay, C. Roubal, et al., "Qualification of inter-satellite link laser communication terminals on CubeSats CubeISL" 37th Small Satellite Conference, (2024).
- [23] R. Rüddenklau, L. R. Rodeck, H. Zeihsel, "Trajectory Control of a Gimbaled Prism for Hemispherical Pointing in CubeSat Optical Communications", (2025) (to be published).